CHEMISTRY OF MATERIALS
Article

Chem. Mater. **2010,** *22,* 3133–3142 3133
DOI:10.1021/cm100061n

Palladium Catalysts Synthesized by Atomic Layer Deposition for Methanol Decomposition

Hao Feng,[†] Jeffrey W. Elam,*[,‡] Joseph A. Libera,[‡] Worajit Setthapun,[†] and Peter C. Stair[†,§]

[†]*Chemical Sciences and Engineering Division, and* [‡]*Energy Systems Division, Argonne National Laboratory, Argonne, Illinois 60439, and* [§]*Department of Chemistry and Center for Catalysis and Surface Science, Northwestern University, Evanston, Illinois 60201*

Received January 7, 2010. Revised Manuscript Received March 22, 2010

Atomic layer deposition (ALD) palladium films were deposited at 200 °C on various ALD metal oxide surfaces using sequential exposures to Pd(II) hexafluoroacetylacetonate ($Pd(hfac)_2$) and formalin. In situ quartz crystal microbalance measurements as well as ex situ measurements performed on planar substrates revealed that the Pd growth begins with a relatively slow nucleation process and accelerates once an adequate amount of Pd has deposited on the surface. Furthermore, the Pd nucleation is faster on ALD ZnO surfaces compared to ALD Al_2O_3 surfaces. ALD was utilized to synthesize highly dispersed, uniform Pd nanoparticles (1 to 2 nm in diameter) on ALD ZnO and Al_2O_3 coated mesoporous silica gel, and the catalytic performances of these samples were compared in the methanol decomposition reaction. The ALD Pd−Al_2O_3 showed high activity and hydrogen selectivity at relatively low temperatures while the ALD Pd−ZnO showed very low activity as well as quick deactivation. In situ extended X-ray absorption fine structure (EXAFS) measurement revealed that the Pd supported on ZnO "dissolves" into the substrate during the methanol decomposition reaction which accounts for the gradual disappearance of its catalytic activity. By applying one cycle of ALD Al_2O_3 on top of the Pd−ZnO catalyst, the activity was enhanced and the catalyst deactivation was mitigated. This Al_2O_3 overcoating method stabilizes the Pd−ZnO and effectively prevents the dissolution of Pd into the ZnO substrate.

Introduction

The low temperature decomposition of methanol to form carbon monoxide and hydrogen may provide a valuable source of hydrogen for use as a transportation fuel.[1] Pd metal is one of the most active species for catalyzing this process.[2−10] Consequently, the mechanism for Pd-catalyzed methanol decomposition has been extensively studied in model catalytic systems over Pd single crystals under ultra high vacuum (UHV) conditions as well as over supported Pd catalysts under atmospheric or higher pressures in the temperature range of 150−400 °C.[11−14] For practical applications, it is cost-effective to utilize this precious metal in a highly dispersed form such as isolated nanoparticles. Furthermore, to make a useful catalyst, it is necessary to apply the Pd nanoparticles onto a high surface area substrate. In recent years, atomic layer deposition (ALD) has emerged as an effective technology for applying precise, conformal thin films onto high surface area substrates such as anodic aluminum oxide membranes[15] and mesoporous silica gel.[16] In the ALD process, two gaseous precursors are pulsed alternately such that each reacts with the surface functional groups generated during the previous pulse to produce a deposition cycle.[17] Since the initial surface functional groups are regenerated at the end of each deposition cycle, this technique is capable of preparing thin films of virtually any thickness with atomic-level precision. In addition

*Corresponding author. E-mail: jelam@anl.gov.

(1) Wilson, M. S. *Int. J. Hydrogen Engine* **2009**, *34*, 2955–2964.
(2) Panel on New Directions in Catalytic Science and Technology, Board on Chemical Sciences and Technology, National Research Council. *Catalysis Look to the Future*; National Academy Press: Washington, DC, 1992.
(3) Wickham, D. T.; Logsdon, B. W.; W., C. S.; Butler, C. D. *J. Catal.* **1991**, *128*, 198–209.
(4) Shiozaki, R.; Hayakawa, T.; Liu, Y.; Ishii, T.; Kumagai, M.; Hamakawa, S.; Suzuki, K.; Itoh, T.; T., S.; Takehira, K. *Catal. Lett.* **1999**, *58*(2−3), 131–140.
(5) Kapoor, M. P.; Chihashi, Y.; J., S. W.; Matsumura, Y. *Catal. Lett.* **2001**, *3*−*4*(76), 139–142.
(6) Matsumura, Y.; Okumura, M.; Usami, Y.; Kagawa, K.; Yamashita, H.; Anpo, M.; Haruta, M. *Catal. Lett.* **1997**, *44*, 189–191.
(7) Liu, Y.; Suzuki, K.; Hamakawa, S.; Hayakawa, T.; Murata, K.; Ishii, T.; Kumagai, M. *Chem. Lett.* (*Chem. Soc. Jpn.*) **2000**, 486–487.
(8) Liu, Y.; Suzuki, K.; Hamakawa, S.; Hayakawa, T.; Murata, K.; Ishii, T.; Kumagai, M. *Catal. Lett.* **2000**, *66*, 205–213.
(9) Usami, Y.; Kagawa, K.; Kawazoe, M.; Matsumura, Y.; Sakurai, H.; Haruta, M. *Appl. Catal., A* **1998**, *171*, 123–130.
(10) Lee, C.; Yoon, H.-K.; Moon, S.-H.; Yoon, K. J. *Korean J. Chem. Eng.* **1998**, *15*(6), 590–595.
(11) Rodriguez de la Fuente, O.; Borasio, M.; Galletto, P.; Rupprechter, G.; Freund, H.-J. *Surf. Sci.* **2004**, *566*−*568*, 740−745.
(12) Matsumura, Y.; Shen, W. J. *Top. Catal.* **2003**, *22*(3−4), 271–275.
(13) Hara, S.; Xu, W. C.; Sakaki, K.; Itoh, N. *Ind. Eng. Chem. Res.* **1999**, *38*, 488–492.
(14) Liu, Y.; Hayakawa, T.; Ishii, T.; Kumagai, M.; Yasuda, H.; Suzuki, K.; Hamakawa, S.; Murata, K. *Appl. Catal., A: General* **2001**, *210*, 301–314.
(15) Stair, P. C.; Marshall, C.; Xiong, G.; Feng, H.; Pellin, M. J.; Elam, J. W.; Curtiss, L.; Iton, L.; Kung, H.; Kung, M.; Wang, H.-H. *Top. Catal.* **2006**, *39*, 181–186.
(16) Libera, J. A.; Elam, J. W.; Pellin, M. J. *Thin Solid Films* **2008**, *516* (18), 6158–6166.
(17) Ritala, M.; Leskela, M. *Handbook of Thin Film Materials*; Academic Press: San Diego, 2001; Vol. *1*.

© 2010 American Chemical Society

to continuous thin films, ALD is also capable of preparing highly dispersed nanoparticles.[18] By selecting the appropriate precursors, a wide range of materials can be prepared by ALD.[17] This unique combination of attributes makes ALD an attractive technology for synthesizing catalysts.[19]

It is generally difficult to achieve thin, continuous noble metal films by ALD on oxide surfaces due to the slow chemisorption kinetics of the ALD metal precursor, the lack of effective reducing agents, and the diffusion and sintering of the noble metal species. Typically, thin ALD noble metal deposits consist of islands or agglomerates. For Pd in microelectronic applications, these problems have been circumvented by first applying a self-assembled monolayer or noble metal seed layer[20,21] or using hydrogen radicals as the reducing agent.[22] These techniques are impractical for catalysis since the seed layers might compromise the catalytic performance and hydrogen radicals recombine too rapidly on surfaces to allow the coating of porous substrates. However, as mentioned above, conformal Pd films are actually undesirable for practical catalysts and the natural tendency for ALD Pd to form nanoparticles is advantageous.

In methanol decomposition, the activity of Pd catalysts depend strongly on the underlying support material. Usami et al. reported that the catalytic activity decreased in the following sequence for Pd catalysts on different supports: Pd−ZrO_2 > Pd−Pr_2O_3 > Pd−CeO_2 > Pd−Fe_3O_4 > Pd−TiO_2 > Pd−SiO_2 > Pd−ZnO.[9] Traditional methods for comparing the activity of the same catalytic species on different supports are not ideal, since the supports are usually synthesized by different methods, and often have different physical properties such as surface area, pore size distribution, or particle size. These factors can affect the catalyst loading and performance. In contrast, ALD is capable of coating a variety of materials, including some of the most commonly used catalyst substrates. In this manner, ALD can be used to tune the catalyst support composition without influencing the surface area or porosity in order to isolate the effect of the support material chemistry on the catalyst performance.

Previously, the ALD of Pd has been examined on Al_2O_3 surfaces using alternating exposures to Pd(II) hexafluoroacetylacetonate ($Pd(hfac)_2$) and formalin.[23] In this paper, we explore the effect of the underlying support chemistry on the Pd nucleation and growth using $Pd(hfac)_2$ and formalin. Furthermore, we investigate the catalytic performance of the ALD Pd supported on different metal oxide layers in the methanol decomposition reaction. Starting with high surface area, mesoporous silica gel, we apply an ALD Al_2O_3 or ZnO support layer followed by the ALD Pd and we characterize these materials using a variety of techniques. Next, we compare the catalytic performance of the ALD Pd supported on ZnO and Al_2O_3 as well as the effect of overcoating the Pd−ZnO with ALD Al_2O_3. Finally, we explain the differences in catalytic behavior between the Pd−Al_2O_3 and Pd−ZnO systems using in situ extended X-ray absorption fine structure measurements.

Experimental Section

The ALD synthesis was carried out in a viscous flow reactor.[24] Ultra high purity nitrogen (Airgas, 99.999%) was used as the carrier gas. Layer-by-layer growth of the catalyst support materials (Al_2O_3 or ZnO) and the Pd catalysts were achieved by alternately exposing the substrates to the precursors and the purge gas using specific timing sequences. ALD timing sequences can be expressed as t1-t2-t3-t4 where t1 and t3 are the exposure times for the two precursors and t2 and t4 are the nitrogen purge times between precursor exposures. The typical precursor exposure and purge times for depositing films on flat substrates are a few seconds. Much longer precursor exposure and purge times (tens to hundreds of seconds) are required for coating high surface area substrates.[16] The precursors used to prepare Al_2O_3 films were trimethyl aluminum (TMA, Aldrich, 99%) and deionized water while the ALD ZnO films used diethyl zinc (DEZ, Aldrich, 99%) and deionized water. Palladium hexafluoroacetylacetate ($Pd(hfac)_2$, Aldrich, 99.9%) and formalin (Aldrich, 37% HCOH and 15% CH_3OH in aqueous solution) were used to deposit Pd thin films and to synthesize supported Pd catalysts. Silicon wafers exposing the [100] surface were used to study the nucleation and growth of Pd on ALD Al_2O_3 and ZnO surfaces. Quartz Crystal Microbalance (QCM) studies were performed during Pd ALD using a Maxtek BSH-150 bakeable sensor, AT-cut quartz sensor crystals (Colorado Crystal Corporation), and a Maxtek TM400 film thickness monitor. The QCM mass measurements were converted to Pd film thicknesses assuming a density for Pd of 12.0 g/cm^3. The supported ALD catalysts were synthesized starting from silica gel (Silicycle S10040M) with a specific surface area of 99.6 m^2/g, a primary particle size of 75−200 μm, and a nominal pore diameter of 30 nm. The ALD reaction conditions for depositing the different materials are listed in Table 1a,b.

The quantity of ALD Al_2O_3 and ZnO deposited on the silica gel was determined by weight gain measured with an analytical balance. X-ray fluorescence spectroscopy (XRF) was used as a nondestructive method to characterize the amount of Pd supported on the Al_2O_3 or ZnO coated silica gel. The XRF spectra were measured with an Oxford ED2000 instrument, and quantification was obtained using Pd K-lines. The XRF data were calibrated by inductively coupled plasma (ICP) measurements taken with a Varian Vista-MPX instrument.

The topologies of the ALD Pd films were studied with a Hitachi S4700 scanning electron microscope (SEM) with a field emission gun electron beam source. Energy dispersive X-ray analysis (EDAX)

(18) Christensen, S. T.; Elam, J. W.; Rabuffetti, F. A.; Ma, Q.; Weigand, S. J.; Lee, B.; Seifert, S.; Stair, P. C.; Poeppelmeier, K. R.; Hersam, M. C.; Bedzyk, M. J. *Small* **2009**, *5*(6), 750–757.
(19) Haukka, S.; Lakomaa, E. L.; Suntola, T. *Adsorption and its application in industry and environmental protection*; Elsevier: New York, 1999; Vol. *120*.
(20) Kim, Y.-S.; Ten Eyck, G. A.; Ye, D. J., C.; Karabacak, T.; Shin, H.-S.; Senkevich, J. J.; Lu, T.-M. *J. Electrochem. Soc.* **2005**, *152*(6), 376–381.
(21) Senkevich, J. J.; Tang, F.; Rogers, D.; Drotar, J. T.; Jezewski, C.; Lanford, W. A.; Wang, G. C.; Lu, T.-M. *Chem. Vap. Deposition* **2003**, *9*(5), 258–264.
(22) Ten Eyck, G. A.; Senkevich, J. J.; Tang, F.; Liu, D.; Pimanpang, S.; Karaback, T.; Wang, G.-C.; Lu, T.-M.; Jezewski, C.; Lanford, W. A. *Chem. Vap. Deposition* **2005**, *11*(1), 60–66.
(23) Elam, J. W.; Zinovev, A.; Han, C. Y.; Wang, H. H.; Welp, U.; Hryn, J. N.; Pellin, M. J. *Thin Solid Films* **2006**, *515*, 1664–1673.
(24) Elam, J. W.; Groner, M. D.; George, S. M. *Rev. Sci. Instrum.* **2002**, *73*(8), 2981–2987.

Table 1. ALD Conditions for Film Deposition on Silicon Wafers (a) and for Catalyst Preparation on Silica Gel Particles (b)

ALD material	nitrogen flow (sccm)	timing sequence t1-t2-t3-t4 (s)	tempera-ture (°C)	system pressure (Torr)	metal precursor partial pressure (Torr)
		1a			
Al_2O_3	360	1-5-1-5	200	1.0	0.3
ZnO	360	1-5-1-5	200	1.0	0.3
Pd	360	2-2-1-2	200	1.0	0.01
		1b			
Al_2O_3	150	60-60-60-60	200	1.0	0.3
ZnO	150	60-60-60-60	150	1.0	0.3
Pd	150	x-x-x-x[a]	200	1.0	0.02

[a] $x = 100-600$ for exploratory studies; $x = 400$ for catalysts tested in methanol decomposition.

was performed on a cross-section of ALD Pd catalysts using the same instrument. The size and shape of ALD Pd nanoparticles supported on the silica gel were studied using a JEOL JEM2010 STEM/TEM.

After depositing the support layer and the Pd catalyst, the samples were tested for the methanol decomposition reaction without further treatment. The catalytic experiments were carried out in a stainless steel micro flow reactor with an inside diameter of ~4 mm. Prior to performing the measurements, the reactor was passivated by coating with 50 nm of ALD Al_2O_3 to reduce interference from background reactions. Ten milligrams of catalyst was used in each experiment. The catalyst was held in the middle of the reactor by a plug of quartz wool. A K-type thermocouple was positioned inside the reactor, in contact with the catalyst layer to measure the reaction temperature. Methanol vapor was introduced into the reaction system using an argon (Airgas, 99.99%) gas bubbler. The bubbler was immersed in an ice−water bath to generate an argon stream with ~4% methanol. Pure argon was used as the balance gas. Most catalytic experiments were performed in the temperature range of 170−300 °C with a gas flow rate of 10 sccm at atmospheric pressure. Reaction products were analyzed by a HP 5890 gas chromatograph equipped with a thermal conductivity detector (TCD). Signals from the TCD were calibrated using certified standard gas mixtures (Scotty, 1.00% CO_2, 0.999% CO, 1.00% H_2, 0.998% CH_4, balance of nitrogen).

Extended X-ray absorption fine structure (EXAFS) measurements were conducted at the insertion-device beamline of the Materials Research Collaborative Access Team (MR-CAT) at the Advanced Photon Source located at Argonne National Laboratory. All EXAFS measurements were performed in transmission mode with ionization chambers optimized for the maximum current at linear response (~10^{10} photons detected/s). The electron beam was calibrated to Pd K edge (24.350 keV). A continuous-flow reactor was used during the in situ EXAFS measurements. The reactor consisted of a quartz tube (1 in. OD, 10 in. length) in which ~50 mg of catalyst was pressed into a cylindrical sample holder. The EXAFS spectra were obtained under He flow at room temperature and 4% H_2/He (100 mL/min) at 250 °C. After measuring the spectra, the reduced catalysts were exposed to a mixture of 4% CH_3OH/He at 250 °C (50 mL/min). Subsequently, the reactor was purged with He, cooled to room temperature, and EXAFS spectra were recorded. WINXAS 3.1 software was used to extract EXAFS data. Coordination parameters were obtained by least-squares fitting of the k^2 weighted Fourier transform of EXAFS oscillations.

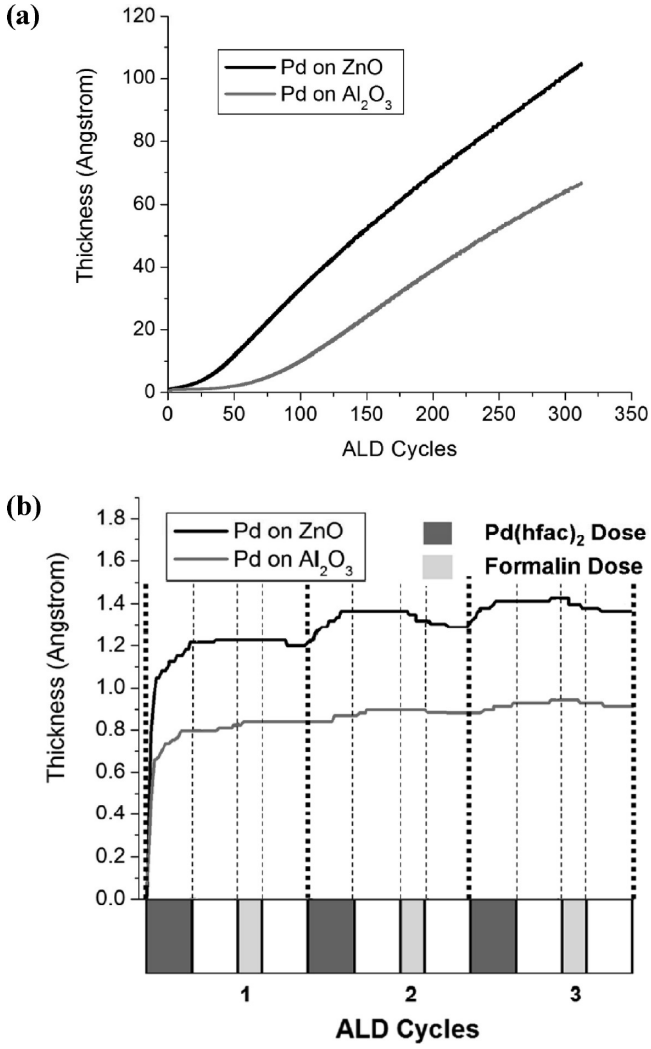

Figure 1. QCM measurements recorded during Pd ALD on ZnO and Al_2O_3 surfaces. (a) QCM data over 300 cycles of Pd ALD. (b) QCM data during the first few Pd ALD cycles.

Results and Discussion

Pd ALD on ZnO and on Al_2O_3 Surfaces. In order to achieve a better understanding of ALD Pd catalyst synthesis, we first investigated the nucleation and growth of ALD Pd films on planar substrates coated with 2 to 3 nm ALD Al_2O_3 and ZnO support layers. QCM measurements of Pd deposited on Al_2O_3 or ZnO are displayed in Figure 1. The plots clearly show that the Pd film growth on both substrates has an incubation period. This phenomenon is observed in many noble metal ALD processes, including the deposition of Pd, Pt, Ru, and Ir on various metal oxide substrates.[20,21,23,25−28] The incubation period may result from surface poisoning by hexafluoro-acetylacetonate (hfac) species.[23,29] As shown in

(25) Aaltonen, T.; Ritala, M.; Sajavaara, T.; Keinonen, K.; Leskela, M. *Chem. Mater.* **2003**, *15*(9), 1924–1928.
(26) Elam, J. W.; Zinovev, A. V.; Pellin, M. J.; Comstock, D. J.; C., H. M. *ECS Trans.* **2007**, *3*(15), 271–278.
(27) Park, S.-J.; Kim, W.-H.; Lee, H.-B.; Wang, W. J.; Kim, H. *Microelectron. Eng.* **2008**, *85*(1), 39–44.
(28) Hamalainen, J.; Puukilainen, E.; Kemell, M.; Costelle, L.; Ritala, M.; Leskela, M. *Chem. Mater.* **2009**, *21*, 4868–4872.
(29) Goldstein, D. N.; George, S. M. *Appl. Phys. Lett.* **2009**, *95*, 143106.

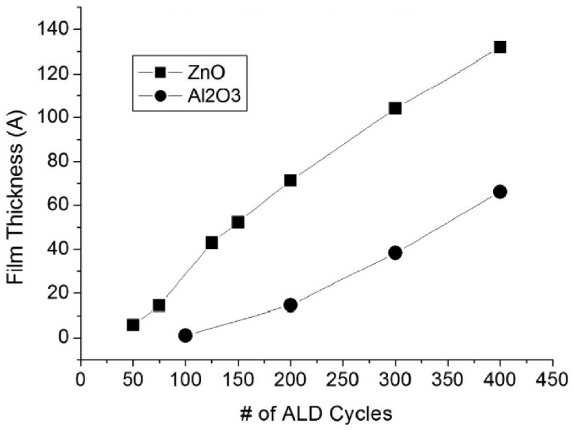

Figure 2. Thicknesses of ALD Pd films deposited on ZnO and on Al_2O_3 measured by XRF.

Figure 1a, the incubation period during Pd ALD is much longer on Al_2O_3 than on ZnO. Approximately 100 ALD cycles were required to reach steady state growth on the Al_2O_3 while only ~30 cycles were required on ZnO. Once steady state growth was achieved, the rates were similar for both substrates.

To further characterize the Pd ALD on the Al_2O_3 and ZnO surfaces, XRF was employed to measure the total amount of Pd deposited on planar substrates of known area. The Pd XRF signals were converted into Pd film thicknesses using a Pd film of known thickness as determined by cross-sectional SEM. Figure 2 shows the Pd film thicknesses measured by XRF after different numbers of Pd ALD cycles deposited on ALD Al_2O_3 and ZnO. The XRF measurements in Figure 2 agree very well with the QCM measurements in Figure 1a. From these plots, we can conclude that the steady state film growth rate is reached once a ~1 nm thick Pd film has been deposited.

SEM images of the Pd films deposited on Al_2O_3 and ZnO are shown in Figure 3. The ALD Pd films begin from isolated islands. As more cycles of Pd ALD are performed, the islands grow until they merge to form a continuous film.[23] The images demonstrate that the nucleation of Pd on ZnO is much faster than on Al_2O_3. One hundred ALD Pd cycles on ZnO yields Pd islands with ~10 to 20 nm domains; at 200 cycles, these domains connect to form a continuous film. However, no Pd islands can be observed by SEM for 100 cycles of Pd deposited on Al_2O_3; as many as 200 cycles were required to form visible islands consisting of ~10 nm domains on the Al_2O_3.

In Pd ALD, the difficulty of removing the hfac ligands after the metal precursor exposure is believed to be the major cause for the low initial growth rate.[23,26] Figure 1b shows the QCM data during the first few cycles of Pd ALD on the surfaces of ZnO and Al_2O_3. On both substrates, the magnitude of the initial $Pd(hfac)_2$ adsorption is similar and the initial thickness change during the first ALD cycle is quite large compared to the subsequent cycles. More thickness loss (corresponding to hfac removal) is observed during the first formalin exposure on ZnO as compared to Al_2O_3. Starting from the second cycle, larger thickness increases during the Pd precursor exposures followed by larger thickness decreases during the formalin exposures can be observed on ZnO; as a result, a larger net thickness is achieved on ZnO for each deposition cycle. This difference may reflect a lesser degree of surface poisoning by hfac ligands on the ZnO surface compared to the Al_2O_3 surface.[29] In addition to the ALD ZnO and Al_2O_3 results shown in Figure 2, we also investigated Pd ALD on ALD MgO and SrO surfaces. XRF measurements of these samples revealed that the nucleation and growth of ALD Pd on the MgO and SrO surfaces are similar to Al_2O_3 (data not shown).

We explored a number of approaches to accelerate the nucleation of Pd ALD including ozone treatment, performing the formalin exposures at a higher temperature (300 °C), longer formalin exposures, longer N_2 purging times, and combinations of these methods. We found that only longer formalin exposures significantly enhanced the rate of ALD Pd nucleation. During the first ALD Pd cycle, a 600 s formalin exposure was applied after an initial $Pd(hfac)_2$ precursor exposure and N_2 purge with the standard timing sequence, followed by a second N_2 purge of 100 s. After the first Pd ALD cycle, the subsequent cycles were performed with the standard timing sequence (2-2-1-2s). The Pd film thicknesses on Al_2O_3 measured by XRF were 10.5 Å for the 100-cycle sample and 39.0 Å for the 200-cycle sample. Compared to the Pd film thicknesses deposited using the standard ALD timing sequence (0.8 Å following 100 cycles and 15.2 Å following 200 cycles), the long initial formalin exposure effectively accelerates the Pd nucleation on Al_2O_3. Consistent with this observation, Figure 3e is an SEM image of a 100-cycle Pd film deposited on Al_2O_3 using the long initial formalin exposure. Pd domains of ~10 nm are easily observed in this image. By comparison, no such domains are seen in Figure 3c which is an identical Pd film prepared without the long initial formalin exposure. Since the first few cycles of Pd ALD occur primarily on the bare metal oxide surface, the longer formalin exposure may remove more of the hfac ligands bound to the Al_2O_3 surface providing a cleaner oxide surface for Pd ALD in subsequent ALD cycles, thereby accelerating the nucleation. It is worth noting that the long formalin exposure only needs to be performed during the first ALD cycle to significantly enhance the Pd nucleation. The same technique may be useful for accelerating film nucleation in other metal ALD systems where the deposition is inhibited by metal oxide-bound ligands that poison the surface.

Synthesis and Characterization of ALD Pd Catalysts. Supported Pd catalysts were synthesized by ALD on high surface area substrates. The ability of ALD to coat high aspect ratio structures allows considerable flexibility in the choice of substrates. Silicycle S10040 M silica gel was selected because its physical and chemical properties are suitable as a practical catalyst support. The precursor partial pressures and exposure times were increased to saturate the much larger surface area of the silica gel as compared to the planar substrates and also to ensure sufficient time for the precursors to infiltrate the porous material. The silica gel was first coated using 5 cycles of

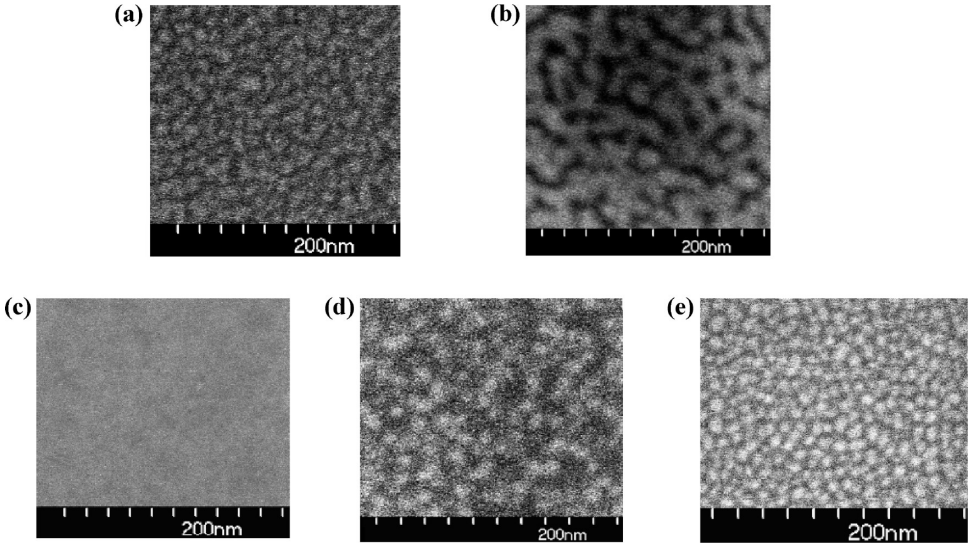

Figure 3. SEM images of ALD Pd films prepared on different substrates: (a) 100-cycle Pd−ZnO, (b) 200-cycle Pd−ZnO, (c) 100-cycle Pd−Al_2O_3, (d) 200-cycle Pd−Al_2O_3, and (e) 100-cycle Pd−Al_2O_3 with long formalin exposure during the first cycle.

ALD Al_2O_3 or 3 cycles of ALD ZnO using a the timing sequence 60-60-60-60 to form the catalyst support layer. The weight gains produced by the support layer depositions were 12.6% for Al_2O_3 and 20.8% for ZnO which corresponds to a thickness of ~0.5 nm for both materials. The Brunauer-Emmett-Teller (B.E.T.) surface area decreased by less than 3% as a result of the support layer coatings.

Next, 1 to 2 Pd ALD cycles were performed to generate ALD Pd catalysts supported on Al_2O_3 (Pd−Al_2O_3) and ZnO (Pd−ZnO). These experiments used the timing sequence *x*-*x*-*x*-*x* where *x* was varied from 100 s to 600 s. Consequently, both the $Pd(hfac)_2$ and the formalin exposure times as well as the purge times were varied. Following the Pd ALD, the sample color changed from white to black, indicating the reduced Pd^0 species. Furthermore, the Pd ALD resulted in a weight gain of 1−3% depending on the substrate, the timing sequence, and the number of ALD Pd cycles performed. The Pd loading was measured by XRF/ICP, and the results are presented in Figure 4. Figure 4 demonstrates that for all of the samples the Pd loading increases steeply for the first ~100 s before achieving a gradual saturation for precursor exposure times exceeding ~200 s. From the partial pressure of the $Pd(hfac)_2$ precursor and the surface area of the silica gel, we calculate a minimum exposure time of ~80 s to saturate the silica gel with 1 Pd/nm^2. In contrast, the minimum exposure time required for the precursors to infiltrate silica gel particles is estimated to be ~190 s, assuming a Knudsen diffusion model.[30] This value is closer to the experimentally observed minimum exposure time in Figure 4, suggesting that precursor diffusion is the rate limiting step in the Pd coating. The Pd uptake was larger during the first Pd ALD cycle than during the second cycle, in agreement with the QCM and XRF results on planar substrates. However, in contrast to our findings on the planar surfaces,

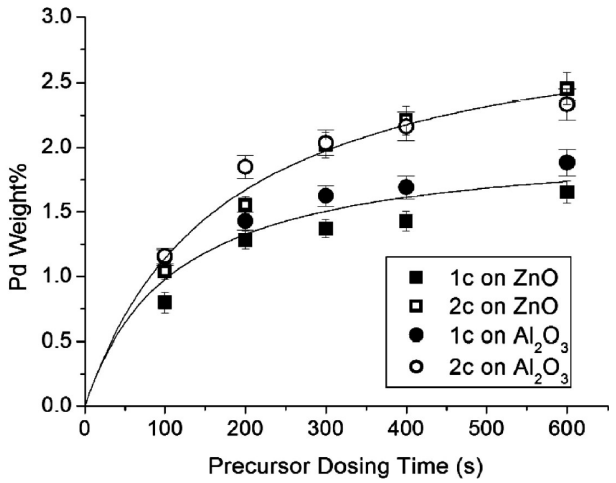

Figure 4. Pd loading on ZnO or Al_2O_3 coated silica gel at different precursor dosing times. The error bars represent the variation in Pd loading measured on duplicate samples. The solid curves present the fittings of the 1 cycle and 2 cycle Pd samples using a Langmuir adsorption model. The average loading of the Pd−ZnO and Pd−Al_2O_3 samples are used in the fittings.

the Pd loading was not significantly different on Al_2O_3 and ZnO for the porous supports. The much longer precursor exposures utilized in coating the high surface area silica gel may enhance the Pd nucleation, thereby eliminating the effect of the different surface chemistries of the ZnO and Al_2O_3 on the Pd ALD.

The spatial distribution of Pd species inside the silica gel particles was characterized by EDAX mapping. To provide sufficient Pd signal for EDAX measurements, samples were prepared with as many as 10 ALD Pd cycles resulting in a Pd loading of ~13%. Next, the silica gel was gently crushed using a spatula to expose cross sections of the coated particles. Figure 5a shows the SEM image of an exposed cross-section from a crushed silica gel particle. Figure 5b,c,d displays the 2-D distribution of Si, Al, and Pd elements in this image measured by EDAX mapping. The signals from Al look very similar to those from

(30) Elam, J. W.; Routkevitch, D.; Mardilovich, P.; George, S. M. *Chem. Mater.* **2003**, *15*, 3507–3517.

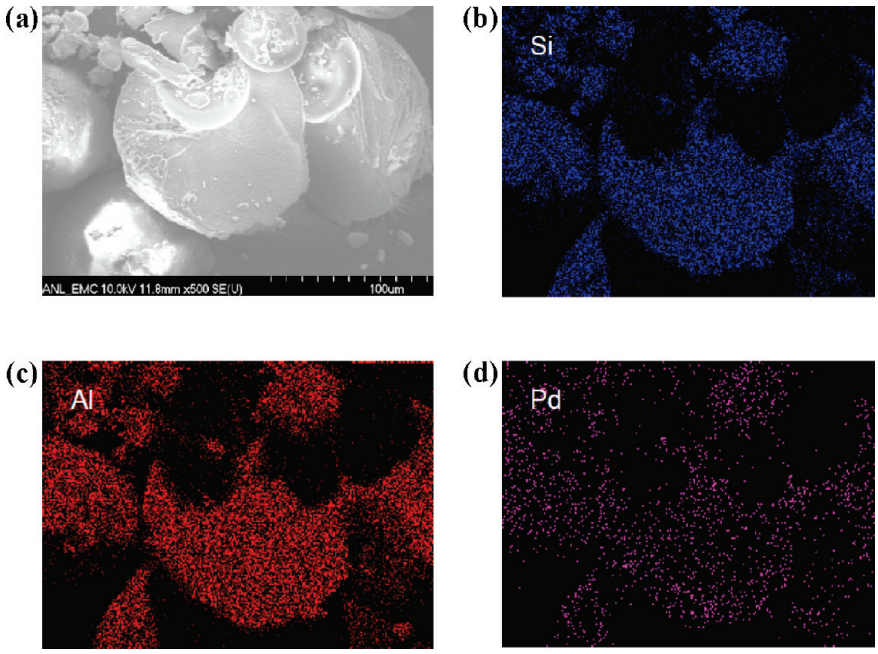

Figure 5. EDAX mapping (combined with the SEM image) of the cross-section of a cleaved silica gel particle: (a) SEM image of the cross-section, (b) EDAX mapping of Si, (c) EDAX mapping of Al, and (d) EDAX mapping of Pd.

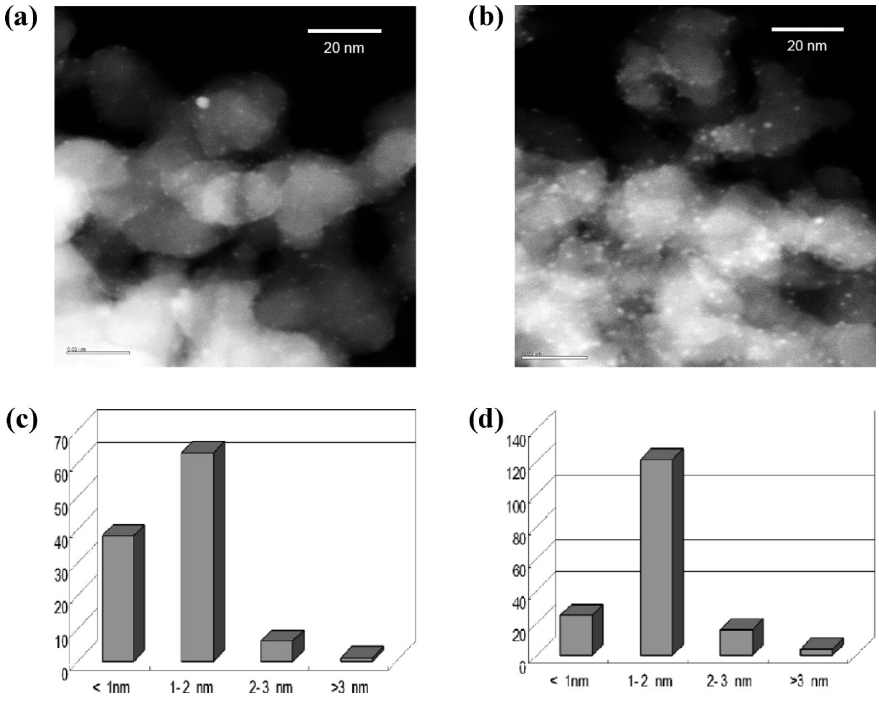

Figure 6. TEM image of the 1c Pd supported on Al_2O_3 prepared using 100 s (a) and 400 s (b) precursor exposure times and the Pd particle size distribution (c and d) deduced from these images.

Si indicating a uniform, complete coverage of the silica gel framework by the ALD Al_2O_3. Although the Pd EDAX signals are considerably weaker than those of Al and Si, the Pd distribution is uniform over the cross-section, indicating complete infiltration of the silica gel particle by the ALD Pd.

Due to the strong tendency to form the stable metal−metal bonds, noble metals prepared by ALD almost always agglomerate to form small particles even after only 1 ALD cycle. Transmission electron microscopy (TEM) was utilized to examine the morphology and particle size distribution of the ALD Pd in the silica gel. Figure 6a,b shows TEM images following 1 ALD Pd cycle on Al_2O_3 coated silica gel using exposure times of 100 and 400 s, respectively. The number of Pd particles in these images was counted, and the sizes of these particles were determined by measuring the diameter of each particle against the scale bar in magnified prints of the images. The accuracy of this measurement was limited to ~1 nm due to the uncertainty in locating the particle edges in the images. The size distributions

are presented as the histograms in Figure 6c,d. A majority of the Pd particles in both samples are 1 to 2 nm in diameter. The distribution of Pd particle sizes in each sample is very narrow, and no aggregation of the particles is observed. The data in Figure 4 show an increase in Pd loading of nearly 40% as the precursor exposure times increase from 100 to 400 s. The two TEM images show a larger density of Pd particles in the sample prepared using longer precursor exposure times. However, the average particle size increases only slightly with longer exposures, and more small particles (< 1 nm diameter) are found in the sample prepared using shorter precursor exposures. No significant difference in the Pd particle size is observed between the Pd−Al_2O_3 samples with 1 and 2 Pd ALD cycles. It was not possible to identify Pd nanoparicles by TEM for the Pd−ZnO samples. This is likely due to the formation of Pd−Zn alloys on the ZnO surface, which is revealed by the EXAFS measurements described below.

The EXAFS spectrum of the reduced 1-cycle Pd−Al_2O_3 catalyst produced two distinct peaks at distances of R = 2.0 and 2.5 Å (Figure 7). These two peaks are correlated to metallic Pd. An entirely different spectral shape was observed for the reduced 1-cycle Pd−ZnO catalyst. Well-defined peaks are present at distances of R = 1.6 and 2.1 Å and a shoulder at 2.5 Å. The shoulder is likely due to Pd−Pd neighbors since it is at the same position as the second peak in the Pd−Al_2O_3 spectra. EXAFS fits for both spectra are summarized in Table 3. Only Pd−Pd scattering was present for the Pd−Al_2O_3 sample with a coordination number (N) of 6.2 and a bond distance of 2.76 Å. For the Pd−ZnO sample, Pd−Pd and Pd−Zn N's were 4.0 and 2.3, respectively, with corresponding bond distances of 2.76 and 2.55 Å. Bollmann et al. reported similar bond distances for Pd−Pd scattering at 2.73 Å and Pd−Zn scattering at 2.54 Å for a 2%Pd−2%ZnO−Al_2O_3 catalyst.[31] Additionally, the Pd−ZnO sample has a Pd−Zn to Pd−Pd N ratio of 2. This ratio and the bond distances were indicative of a face-centered tetragonal structure of a 1:1 PdZn intermetallic compound.[31]

As the Pd loading increased from 1 to 2 Pd ALD cycles on Al_2O_3, the coordination number of Pd−Pd neighbors increased only slightly from 6.2 to 6.7. Since Pd particle size is correlated to N, the Pd particle sizes are about the same for these two samples. This is consistent with Pd growth occurring primarily on the Al_2O_3 support during the second cycle, yielding a higher density of particles having approximately the same size between the 1-cycle and 2-cycle Pd−Al_2O_3 samples. This result is in agreement with the conclusions from TEM measurements. These results indicate that in the first few cycles of Pd ALD it is the adsorption of the Pd precursor onto the bare oxide surface that determines the amount of Pd that can be deposited in each cycle. Therefore, removing the hfac ligands which poison the support is the critical factor affecting the Pd growth per cycle. As for the Pd−ZnO materials, the ratios of N for Pd−Zn to Pd−Pd were 1.7 and 2.8 for 1-cycle Pd−ZnO and 2-cycle Pd−ZnO catalysts, respectively. The larger fraction of Pd−Zn neighbors present in 2-cycle Pd−ZnO suggests that the second cycle of Pd may be deposited on the support and incorporated with ZnO.

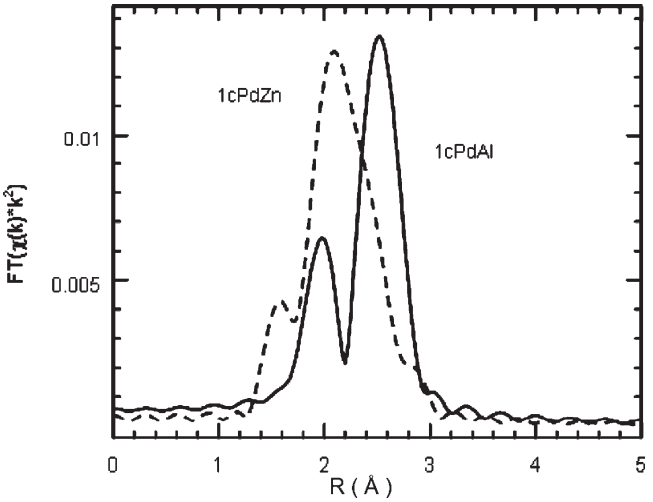

Figure 7. EXAFS fitting of the Pd−Al_2O_3 and Pd−ZnO catalysts after hydrogen treatment at 250 °C.

Table 2. Product Distribution of the 1-Cycle Pd−Al_2O_3 and 1-Cycle Pd−ZnO in Methanol Decomposition

	1- cycle Pd−Al_2O_3 selectivity (%)		1-cycle Pd−ZnO selectivity (%)		
	CO	CH_4	CO	CO_2	$HCOOCH_4$
190 °C	100	0	99.4	0.1	0.5
230 °C	99.2	0.8	83.3	9.2	7.5
270 °C	98.7	1.3	64.8	16.2	19.0

Catalytic Performance of ALD Pd−Al_2O_3 and Pd−ZnO in Methanol Decomposition. The catalytic performance of the Pd−Al_2O_3 and Pd−ZnO samples was studied for the methanol decomposition reaction in the temperature range of 160−300 °C. In all tests, the catalytic activity and selectivity measured for duplicate samples prepared with the same composition and having the same history is reproducible within 5%. Blank experiments were performed on silica gel samples with only Al_2O_3 or ZnO coatings. No background reaction was found on the Al_2O_3 coated silica gel at temperatures up to 350 °C. However, on the silica gel coated with ZnO, small amounts (~0.5−1% conversion) of methyl formate were detected at temperatures above 240 °C. Figure 8 plots the conversion curves for the catalysts with 1-cycle and 2-cycle ALD Pd supported on Al_2O_3 and on ZnO as a function of temperature from 160 to 300 °C. Clearly, the support has a dramatic effect on the activity of the catalyst. The Pd−Al_2O_3 catalysts were quite active. At a space velocity of 60 000 mL/h/g-cat (~4% methanol), nearly complete methanol conversion was reached at 280 °C. The catalytic activity of the Pd−Al_2O_3 samples was rather stable with only a ~5% decrease in the activity during the first 6 h of continuous running at 250 °C and essentially constant activity thereafter. On these catalysts, the conversion versus reaction temperature curve was

(31) Bollmann, L.; Ratts, J. L.; Joshi, A. M.; Williams, W. D.; Pazmino, J.; Joshi, Y. M.; Miller, J. T.; Kropf, A. J.; Delgass, W. N.; Ribeiro, F. *J. Catal.* **2008**, *257*(1), 43–54.

Table 3. EXAFS Fitting Results for Coordination Number (N), Bond Distance (R), Debye-Waller Factor (DWF), and Energy Correction Factor (E_0) for Pd Catalysts after Reduction and Methanol Decomposition

		H_2 reduction					methanol decomposition				
catalyst	scatter	N	R	DWF × 10^{-3}	E_0 (eV)	Pd−Zn N−Pd−Pd N	N	R	DWF × 10^{-3}	E_0 (eV)	Pd−Zn N−Pd−Pd N
1cPdAl	Pd−Pd	6.2	2.76	3.0	−2.4		7.6	2.76	3.0	−3.4	
2cPdAl	Pd−Pd	6.7	2.76	3.0	−2.4		7.7	2.76	3.0	−3.1	
1cPdZn	Pd−Zn	4.0	2.55	3.0	−4.9	1.7	6.2	2.56	3.0	−2.6	
	Pd−Pd	2.3	2.72	3.0	−4.0						
2cPdZn	Pd−Zn	4.9	2.55	3.0	−4.0	2.9	6.8	2.57	3.0	−1.6	
	Pd−Pd	1.7	2.72	3.0	−2.0						
1cAl−1cPdZn	Pd−Zn	2.9	2.55	3.0	−4.5	1.0	3.2	2.55	3.0	−4.3	1.3
	Pd−Pd	3.0	2.72	3.0	−2.0		2.5	2.72	3.0	−2.4	
2cAl−1cPdZn	Pd−Zn	2.5	2.55	3.0	−3.2	0.8	2.9	2.55	3.0	−3.5	0.9
	Pd−Pd	3.1	2.72	3.0	−0.9		3.1	2.72	3.0	−0.8	

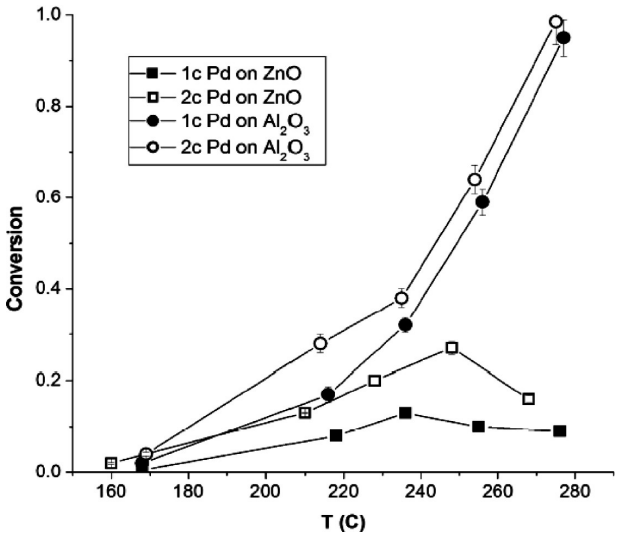

Figure 8. Conversion curves of the ALD Pd−Al_2O_3 and Pd−ZnO catalysts in methanol decomposition.

independent of whether the temperature was ramped up or down. The Pd−ZnO catalysts showed quite different behavior. These catalysts deactivated quickly at temperatures higher than 230 °C. The deactivation was so rapid that, in a series of experiments using a continuous temperature ramp, the conversion began to drop even with the increasing temperature (Figure 8). At 250 °C, the activity of Pd−ZnO decreased by over 80%, and this decrease in activity was irreversible. The type of support also affects the selectivity of the ALD Pd catalysts in methanol decomposition. Table 2 presents the typical product distribution from the two types of catalysts. Under our experimental conditions, both the Pd−Al_2O_3 and Pd−ZnO catalysts produced mostly CO and H_2. The only other product of the Pd−Al_2O_3 catalyst was CH_4, which appeared at temperatures higher than 230 °C and accounted for ≤1% of the selectivity based on carbon. CO_2 and methyl formate were the other products formed by the Pd−ZnO catalysts. These two products are typical for decomposition/steam reforming of methanol over Pd−Zn alloys.[32,33]

The rapid deactivation of the Pd−ZnO catalyst is related to the formation of Pd−Zn alloys during the methanol decomposition reaction. The formation of these Pd−Zn alloys was observed using in situ EXAFS/XANES measurements, in which methanol decomposition was performed at 250 °C under a flow of 4% CH_3OH/He mixture over the reduced Pd−ZnO or Pd−Al_2O_3 catalysts. The spectra were recorded until no change was observed. The samples were then purged at 250 °C and cooled to room temperature. The EXAFS data taken at room temperature are summarized in Table 3. Pd−Pd N for 1-cycle Pd−Al_2O_3 increased to approximately 7.6 from 6.7. A similar increase in N was observed for 2-cycle Pd−Al_2O_3. The increase in N can be attributed to Pd particle sintering during methanol decomposition. For 1-cycle Pd−ZnO and 2-cycle Pd−ZnO, the reduced catalysts contained both Pd−Pd and Pd−Zn scattering. After methanol decomposition, only Pd−Zn scattering was observed with N of 6.2 and 6.8 for 1-cycle Pd−ZnO and 2-cycle Pd−ZnO, respectively. In addition, for the 1-cycle Pd−ZnO, only one peak at R = 2.2 Å was observed, corresponding to Pd−Zn neighbors. No Pd−Pd scattering was detected in the spectra.

The reaction conditions for methanol decomposition appear to facilitate dissolution of Pd into the ZnO. The formation of Pd−Zn alloy in the ZnO supported Pd system has been shown previously by XRD and XPS techniques.[9,34] The alloy formation is favored in reducing environments and with a good dispersion of the Pd species.[34] The Pd−Zn alloy is an active catalyst for methanol steam reforming, producing CO_2 and hydrogen.[33−36] The role of methanol decomposition and the produced CO has been a topic of debate in the mechanism of methanol steam reforming over Pd−Zn systems, since CO could act as an intermediate to produce CO_2 through the water gas shift reaction.[37,38] Another mechanism including methyl formate as intermediate has been proposed by Takahashi and co-workers.[39] By feeding CO together with methanol

(32) Iwasa, N.; Yamamoto, O.; Akazawa, T.; Ohyama, S.; Takezawa, N. *J. Chem. Soc. Chem. Commun.* **1991**, 1322–1323.
(33) Iwasa, N.; Kudo, S.; Takahashi, H.; Masuda, S.; Takezawa, N. *Catal. Lett.* **1993**, *19*, 211–216.
(34) Iwasa, N.; Masuda, S.; Ogawa, N.; Takezawa, N. *Appl. Catal., A* **1995**, *125*, 145–157.
(35) Pfeifer, P.; Kolbl, A.; Schubert, K. *Catal. Today* **2005**, *110*, 76–85.
(36) Bera, P.; Vohs, J. M. *J. Phys. Chem. C* **2007**, *111*, 7049–7057.
(37) Santacesaria, E.; Carra, S. *Appl. Catal.* **1983**, 5.
(38) Amphlett, J. C.; Evans, M. J.; Jones, R. A.; Mann, R. F.; Weir, R. D. *Can. J. Chem. Eng.* **1985**, *63*(4), 605–611.
(39) Takahashi, K.; Takezawa, N.; H., K. *Appl. Catal.* **1982**, *2*(6), 363–366.

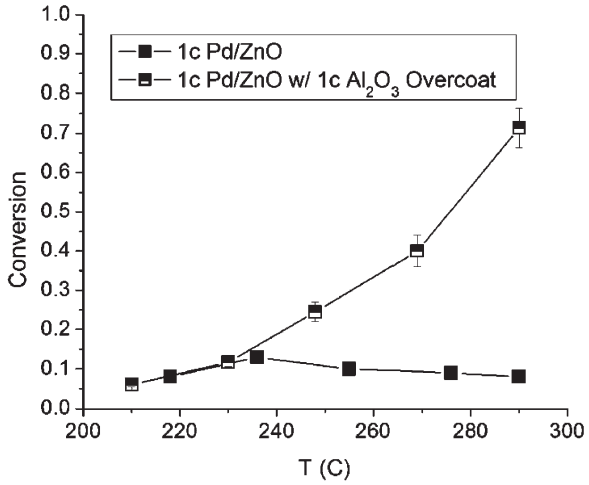

Figure 9. Comparison of the conversions of the ALD Pd−ZnO catalyst in methanol decomposition with and without 1 cycle of ALD Al_2O_3 overcoat.

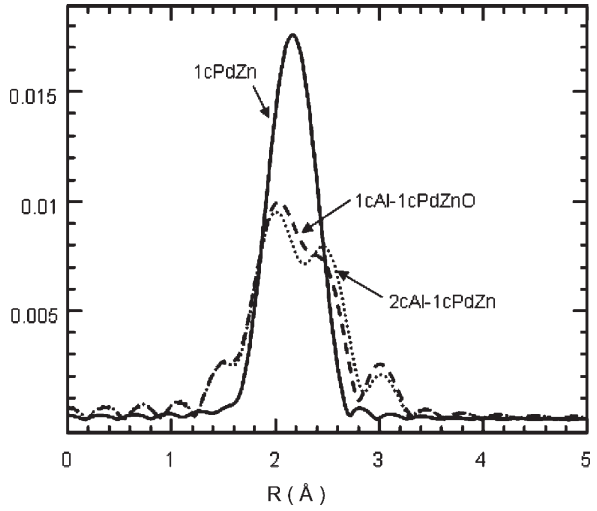

Figure 10. EXAFS fitting of the original Pd−ZnO catalyst and the same catalyst with 1 or 2 cycles of ALD Al_2O_3 overcoat after hydrogen treatment at 250 °C.

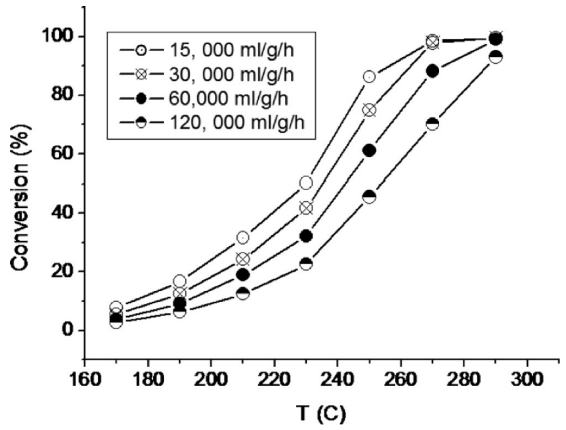

Figure 11. Methanol conversions over the 1-cycle ALD Pd−Al_2O_3 catalyst measured at different space velocities.

and water and analyzing the equilibrium constant K_p of water gas shift reaction, Iwasa et al. claimed that a water gas shift reaction had no contribution to the CO/CO_2 selectivities in methanol steam reforming over the Pd−Zn system and that CO was produced only from the methanol decomposition over Pd^0 sites.[33] With the ALD Pd−ZnO catalysts, the diminishing activity in methanol decomposition with the transition from Pd^0 to Pd−Zn straightforwardly shows that CO is mostly (if not exclusively) produced through methanol decomposition on metallic Pd.

Effect of Alumina Overcoats on the Catalytic Performance of Pd−ZnO Catalysts. Since the dissolution of Pd into the ZnO substrate appears to be the cause of the catalyst deactivation, stable activity might be achieved by preventing the Pd−ZnO interaction. Overcoating the Pd−ZnO catalysts with ALD Al_2O_3 is a convenient and intriguing approach. TMA molecules could potentially react with surface hydroxyls on the ZnO to form a barrier layer between Pd and ZnO. TMA is not likely to react with the supported Pd since OH groups are not present on the Pd, and consequently, the active sites for methanol decomposition would not be blocked by the Al_2O_3 overcoats. The Pd−ZnO catalysts overcoated with 1 or 2 cycles of ALD Al_2O_3 were prepared using the standard preparation conditions listed in Table 1b. In subsequent tests, the Pd−ZnO catalyst with Al_2O_3 overcoats showed greatly improved catalytic performance for the methanol decomposition reaction. The conversion vs temperature of the 1-cycle Pd−ZnO catalyst with 1-cycle Al_2O_3 overcoat and the 1-cycle Pd−ZnO catalyst without overcoating is compared in Figure 9. The Al_2O_3 overcoated catalyst exhibits significantly higher activity. Unlike the regular Pd−ZnO catalyst, the methanol conversion increases continuously with reaction temperature for the overcoated catalyst, and no significant deactivation was observed at 270 °C during 6 h of continuous testing.

In situ EXAFS/XANES measurements were performed on the Pd−ZnO catalysts with Al_2O_3 overcoats, and the results are presented in Figure 10 and Table 3. In Figure 10, peaks at 2.05 and 2.5 Å were observed for both Pd−ZnO samples with 1 and 2 cycles of Al_2O_3 overcoat corresponding to Pd−Zn and Pd−Pd neighbors. The ratio between N of Pd−Zn to Pd−Pd after methanol decomposition reaction conditions for the Pd−ZnO with 1-cycle Al_2O_3 overcoat was 1.3, only slightly higher than the value of 1.0 for the reduced Pd−ZnO catalyst. One cycle of Al_2O_3 overcoating significant inhibited Pd dissolution in Zn during methanol decomposition. Overcoating using 2 cycles of ALD Al_2O_3 further stabilized the Pd−Zn to Pd−Pd N ratio. While the mechanism for this stabilization is not presently understood, it is likely that the Al_2O_3 layer covers exposed ZnO surface and serves as a diffusion barrier to prevent dissolution of Pd into ZnO substrate. These results demonstrate that the addition of inert overcoats using ALD can help stabilize the size and shape of Pd catalyst particles.

Evaluation of ALD Pd−Al_2O_3 Catalysts. The ALD Pd−Al_2O_3 catalysts showed very high activity for the methanol decomposition reaction. Figure 11 presents the conversion for the 1-cycle Pd−Al_2O_3 catalyst at different reactant space velocities. Generally, the conversion decreases with increasing space velocity, and the temperature required for complete

Table 4. Hydrogen Production Rate of the 1-Cycle ALD Pd−Al_2O_3 Catalyst and Some Other Most Active Pd-Based Catalysts Reported in Methanol Decomposition

catalyst	preparation method	H_2 production rate at ~250 °C ($g(H_2)/g(cat)/h$)	Pd loading (weight %)	STY[a] (1/h)	reference
1-cycle Pd−Al_2O_3	ALD	0.39	1.6	1300	this work
Pd−CeO_2−Al_2O_3	sol−gel with $Pd(NO_3)_2$	0.32 (255 °C)	5	340	ref 40
Pd−Mg(Al)O	coprecipitation with $Pd(NO_3)_2$, $Mg(NO_3)_2$, and $Al(NO_3)_3$	0.25	3.6	370	ref 4
Pd−Al_2O_3	incipient wetness impregnation with $PdCl_2$	0.23	2.1	580	ref 10
Pd−ZrO_2	impregnation with $PdCl_2$	0.45 (240 °C)	2.0	1200	ref 6

[a] The space-time yield (STY) is calculated based on the total amount of support Pd.

methanol conversion increases. On this catalyst, 100% conversion is reached below 300 °C at a space velocity as high as 120 000 mL/g/h (~ 4% methanol). Considering the low Pd loading (1.6% by weight) of the ALD Pd−Al_2O_3 catalysts, the specific activity (turn over frequency, TOF based on the total amount of supported metal) is higher than the majority of Pd catalysts synthesized by other methods reported in literature. Table 4 lists the hydrogen production rate of the 1-cycle ALD Pd−Al_2O_3 catalyst at a space velocity of 120 000 mL/h/g-cat compared to some of the most active Pd-based catalysts reported for this reaction near 250 °C and in the conversion range of 20−40%.[4,6,10,40] While the reactions in the literature were conducted at different methanol concentrations (4% to 20%), this should not significantly influence the comparison. We examined the influence of methanol (and the produced CO and H_2) partial pressure on the reaction rate at 250 °C in a methanol concentration range between 2% and 15%; the measured reaction rate was nearly independent (within 10%) of the methanol concentration in the feed at low partial pressures. This is in agreement with the results from kinetic studies performed by Shiizaki et. al.[41] Compared to catalysts prepared by conventional methods (sol−gel, wet impregnation, etc.), the ALD catalysts achieve much higher activity with a comparable or lower loading of Pd. This fact is most meaningful for the costly noble metal-based catalytic systems. The Pd−ZrO_2 system showed slightly better activity than ALD Pd−Al_2O_3.[6] Since ZrO_2 has been reported to be a highly effective promoter of Pd for methanol decomposition,[9] the performance of ALD Pd catalysts would very likely be further improved if ZrO_2 was applied as a support or overcoat material.

The excellent catalytic performance of the ALD Pd catalysts is likely due to their ultrauniform dispersion and small particle size. The self-limiting surface reaction attribute of ALD effectively prevents the uneven accumulation of Pd species on the support and, thus, reduces the formation of large particles. Consequently, most of the deposited Pd species are exposed and available for catalytic reactions. In addition to more efficient use of the catalyst, the small size of the Pd nanoparticles may enhance the specific activity for this reaction. Saitoh and co-workers have studied the effects of Pd particle size on the catalytic activities in methanol decomposition on various oxide supports;[42] their results suggest that the TOFs (normalized by the number of active sites measured by CO chemisorption) for Pd species supported on Al_2O_3 increase as the particles become smaller. Since the majority of the ALD Pd−Al_2O_3 catalyst particles are smaller than the particles synthesized by traditional methods, their catalytic activity could be higher, based on a particle size effect. It should be possible to synthesize even smaller ALD Pd clusters by reducing the density of attachment sites for the Pd precursor via suitable surface treatments prior to the Pd ALD. A promising approach to stabilize small Pd nanoparticles is to deposit diffusion barrier layers that reduce the sintering of Pd species. Further exploration of synthesizing and stabilizing ultrasmall (< 1 nm) noble metal catalyst particles using the ALD technique is currently under way.

Conclusions

ALD Pd films were deposited on ALD Al_2O_3 and ZnO coated surfaces using $Pd(hfac)_2$ and formalin as the precursors. The Pd nucleation is faster on the ZnO surface compared to the Al_2O_3 surface, and longer formalin exposures accelerate the Pd nucleation, probably by facilitating the removal of hfac ligands which block sites for subsequent $Pd(hfac)_2$ adsorption. Using the same methods, Pd nanoparticles were synthesized on ALD Al_2O_3 and ZnO coated (~0.5 nm) mesoporous silica gel by increasing the precursor exposures. On this high surface area substrate, Pd saturation was achieved using precursor exposure times larger than ~200 s. EDAX mapping demonstrated that the distribution of Pd species was uniform throughout the silica gel particles. TEM characterization showed that these ALD Pd nanoparticles are highly dispersed on the Al_2O_3 support and have a narrow size distribution in the range of 1 to 2 nm.

The catalytic performance of ALD Pd supported on ZnO and Al_2O_3 was compared in the methanol decomposition reaction. Due to the very high dispersion of the Pd species in the Pd−Al_2O_3 catalysts, the specific activities of these catalysts are exceptionally good. However, the Pd−ZnO catalysts showed very limited activity as well as rapid deactivation. In the Pd−ZnO catalytic system, in situ EXAFS measurements revealed the gradual formation of Pd−Zn bonds during hydrogen reduction and methanol decomposition, indicating that the Pd supported on ZnO can "dissolve" into the substrate causing the catalyst to lose its activity. Overcoating the Pd−ZnO catalyst with one or two cycles of ALD Al_2O_3 can effectively reduce the dissolution of Pd into the ZnO and, thus, maintain the activity of the catalyst.

(40) Brown, C. J.; Gulari, E. *Catal. Comm.* **2004**, *5*, 431–436.
(41) Shiizaki, S.; Nagashima, I.; Y., M.; Haruta, M. *Catal. Lett.* **1998**, *56*, 227–230.
(42) Saitoh, Y.; Ohtsu, S.; Makie, Y.; Okada, T.; Satoh, K.; Tsuruta, N.; Terunuma, Y. *Bull. Chem. Soc. Jpn.* **1990**, *63*(1), 108–115.